Environmental Research 232 (2023) 115927

Contents lists available at ScienceDirect

Environmental Research

journal homepage: www.elsevier.com/locate/envres

Activated ZnCl2 biochar and humic acid as additives in monoammonium phosphate fertilizer: Physicochemical characterization and agronomic effectiveness

Maurício Cunha Almeida Leite [a,*], Fabiane Carvalho Ballotin [b], José Ferreira Lustosa Filho [b], Wedisson Oliveira Santos [c], Patrícia Cardoso Matias [b], Denison Pogorzelski [b], Leonardus Vergutz [d], Edson Marcio Mattiello [b]

[a] Department of Soil Science, Universidade de São Paulo, Piracicaba, Brazil
[b] Department of Soil Science, Universidade Federal de Viçosa, Viçosa, Brazil
[c] Institute of Agricultural Sciences, Universidade Federal de Uberlândia, Uberlândia, Brazil
[d] AgroBiosciences Program, Mohammed VI Polytechnic University (UM6P), Ben Guerir, Morocco

ARTICLE INFO

Handling Editor: Aijie Wang

Keywords:
Phosphate use efficiency
Functionalized biochar
Phosphorus availability
Phosphate release
Organic acids

ABSTRACT

Activated zinc biochar (ZnBC) and humic acid (HA) were used as coating agents in a soluble monoammonium phosphate (MAP) to modify phosphorus (P) use efficiency by altering adsorption/desorption kinetics between the granule region and the soil. The coated treatments MAPZnBC and MAPHA were compared with MAP through P diffusivity, kinetics, and agronomic evaluation. Eucalyptus sawdust was used as biomass for biochar synthesis, and a pre-pyrolysis treatment with zinc chloride ($ZnCl_2$) was applied. The P diffusivity was evaluated in the fertosphere zone. Adsorption and desorption potential of the ZnBC compared with control biochar (BC) was evaluated separately. Desorption kinetics of P from soil was assessed after incubation with MAPZnBC and MAPHA. The shoot dry matter yield (SDM), P uptake, and P use efficiency (PUE) were evaluated with a pot experiment in a clay Oxisol sown with maize and soybeans as successive plant trials, under glasshouse conditions. Surface area values of 940 and 305 $m^2\ g^{-1}$ combined with adsorption capacities of 106 and 53 mg P g^{-1} for ZnBC and BC, respectively, confirm the increased capacity of activated biochar to adsorb P. Both MAPZnBC and MAPHA decreased P diffusivity compared to MAP after 20 days of incubation. Moreover, MAPZnBC and MAPHA presented 20% and 34% more water-soluble phosphorus recovery. MAPZnBC expressed an increase in SDM while MAPHA highlighted P uptake and PUE compared with MAP. Both kinetic studies and agronomic evaluations showed that ZnBC and HA are suitable as coatings for phosphate fertilizers in terms of increasing P efficiency in the fertosphere on high P-fixing soils.

1. Introduction

Phosphorus's supply chain and its essentiality for global food security are beyond doubt. However, there are countries where the phosphate balance (total supply minus total demand) is negative (FAO, 2018). In Brazil, there has been a significant increase in the use of phosphate fertilizers in recent decades (Withers et al., 2018), which has led to a significant contribution to the green revolution in this country. Nevertheless, the phosphorus (P) surplus (P inputs minus P yield) from mineral fertilization in tropical soils is likely to be greater than crop demand (Pavinato et al., 2020). This occurs due to the high P-adsorbing capacity of highly weathered soils, especially for those rich in iron (Fe) and aluminium (Al) (oxy)hydroxides (Novais and Smyth, 1999). These features could lead to a supply risk in the coming decades (Geissler et al., 2019) and even a P scarcity scenario (Zou et al., 2022).

Increasing the ratio between P yield and P inputs by phosphorus use efficiency (PUE), in line with circular economy and sustainability, may be an alternative for this plot for most tropical agriculture. There is an opportunity to utilize new technologies with phosphate fertilizers to enhance P recovery by plants and simultaneously reduce soil P losses (Guelfi et al., 2022). Many forms of controlled release fertilizers (CRFs) to match plant demand with nutrient release have been widely studied

* Corresponding author. Department of Soils, Universidade de São Paulo/ESALQ, Av. Pádua Dias, 11, 13418-900,Piracicaba, SP, Brazil.
E-mail address: cunhamauricio@usp.br (M.C. Almeida Leite).

https://doi.org/10.1016/j.envres.2023.115927
Received 1 January 2023; Received in revised form 11 April 2023; Accepted 15 April 2023
Available online 21 April 2023

in recent years (Rajan et al., 2021). However, knowledge gaps remain in our understanding of how biochar-based fertilizers (BBFs) (Melo et al., 2022) and also fixation inhibitors such as humic acids (HA) (Jing et al., 2020) can enhance P fertilizer granules (Samoraj et al., 2022).

Biochar (BC) is a carbon-rich product obtained by thermochemical degradation under a restricted oxygen supply (Lehmann and Joseph, 2015). As a renewable product and a stable source of carbon, it can be used for enhancing soil carbon stocks (Gross et al., 2021), soil health and productivity (El-Naggar et al., 2018). Biochar can be activated and potentiate its physicochemical features such as surface area, charge density and adsorption capacity (Nguyen et al., 2022). When the chemical activation is performed before pyrolysis, the activating agent acts on the formation of the BC structure (co-pyrolysis), and chemical activation occurs simultaneously with the pyrolysis (Altintig and Kirkil, 2016). Among the options, zinc chloride ($ZnCl_2$) has been widely used as an activator and co-pyrolysis agent for BC synthesis (Ghodszad et al., 2021; Nguyen et al., 2022; Tian et al., 2019). Furthermore, zinc is an essential chemical element for plant nutrition. When applied to soil, functionalized BC has often been reported to increase P recovery by plants (Shi et al., 2023). It may influence P dynamics in soil, through mechanisms such as changes in soil pH (Xu et al., 2014); changing P adsorption and desorption equilibrium acting in the formation of organo-mineral complexes (Gao et al., 2019); altering microbial biomass and enzyme activities in P dissolution (Yang and Lu, 2022); or by changing mycorrhizal associations (Dai et al., 2021).

The term humic substances (HS) refers to a group of heterogeneous and complex structures of organic substances found in soils, peats, natural waters, and sediments (MacCarthy et al., 2015). The difficulty in classifying and grouping so many substances into one category is that it does not include the original plant, animal and microbial cells, but an extracellular secondary synthesis that varies with time, space and environment (Zavarzina et al., 2021). Moreover, the term "humic acid" (HA) represents the fraction of substances within HS that can be partially dissolved by strong bases and reprecipitated after acidification (Yang and Antonietti, 2020). Leonardite is a concentrated form of HA, which is an oxidized structure of lignite, and consists of medium brown, coal-like substances that occur at shallow depths, overlying more compact coal (Della Lucia et al., 2021). The application of HA has been shown to reduce P adsorption while increasing desorption, thereby increasing P plant-available forms in weathered soils (Zhu et al., 2018). Humic acids are classified from the point of view of fertilizer technologies as cation-sequestering agents or blocks (Guelfi et al., 2022). Humic acids also have different roles such as chelating soil nutrients (Sible et al., 2021), increasing soil cation exchange capacity (CEC) (Laskosky et al., 2020) and phosphatase activity of soil microorganisms (Ampong et al., 2022). As a plant biostimulant, HA has the role of stimulating root and shoot growth and even increases photosynthesis and stress resistance of plants (Xu et al., 2021). However, since HA is a material with low total nutrient content, it cannot supply the nutrients requirements in crop production on its own.

Given the significant challenges facing the global phosphate fertilizer market, the reduced use and efficiency of phosphate fertilizers in tropical soils, and the emergence of new technologies in the fertilizer industry, the aim of the current study was to investigate and compare two types of carbon-based coating to reduce P adsorption in the granule region (fertosphere) and increase the use of P by the plants. A Zn activated biochar (ZnBC) was used as a buffer matrix between the phosphate granule and the soil. On the other hand, a humic acid source was used as a blocking agent to reduce P sorption. Both coatings were tested in a soluble mineral phosphate fertilizer (MAP). In addition, the study compared the effectiveness of ZnBC and HA as coatings by quantifying their diffusivity, adsorption/desorption kinetics and their agronomic effect on plant P uptake.

2. Materials and methods

2.1. Biochar production

The BC used in this study was prepared from sawdust of *Eucalyptus* spp. The preparation consisted of oven-dried sawdust (<30 mm) at 105 °C to constant weight. After drying, 200 g of sawdust was impregnated with a $ZnCl_2$ solution (204 g L^{-1} $ZnCl_2$) (sawdust: $ZnCl_2$ mass ratio ~ 1:1), the suspension was stirred at 80 °C for 7 h, and then dried on a heating plate (200 °C) until the liquid evaporated. The biomass impregnated with $ZnCl_2$ was again dried in a closed circulating air oven at 105 °C until it reached a constant weight. The material was then placed in hermetically sealed stainless steel cylinders and placed in a top-opening muffle furnace (Lustosa Filho et al., 2017). Pyrolysis was carried out at 500 °C with a heating rate of 10 °C min^{-1} and a holding time of 1 h. After the production of the control biochar (BC) and zinc-biochar (ZnBC), the material was washed with deionized water until pH and electrical conductivity (EC) remained constant. The end products were ground and passed through an 80-mesh (177 μm) sieve and stored for physicochemical analysis. The HA was obtained from Fertilizantes Heringer S.A. (Minas Gerais, Brazil) and was extracted from leonardite (Alberta, Canada), which is a commercial HA produced by alkaline extraction (0.5 mol L^{-1} KOH).

2.2. Coating of MAP granules

Coated P fertilizers were produced by adding ZnBC or HA to the surface of monoammonium phosphate [MAP - (NH_4) H_2PO_4, a commercial source] granules. Prior to coating, MAP granules were selected by weight (32 ± 0.02 mg) and dried at 50 °C to constant weight. A solution containing water, acetone, agglutination (mucilage, 2.0%) and ZnBC or HA was then pulverized on MAP granules, using a rotary granulator inclined at 45°, as described elsewhere (Pogorzelski et al., 2020). An industrial dryer attached to the granulator was used to ensure that the bulk addition of granules was due to adhering solids and not moisture in the applied solution. At the end of the process, the fertilizers obtained were MAP coated with ZnBC (MAPZnBC) or with HA (MAPHA) at coating ratios of 0.5, 1.0, or 2.0 wt%.

2.3. Characterization of biochar and humic acids

The total concentration of chemical elements (P, K, Ca, S, Mg, Zn, Fe, Al, Si and Ni) in BC, ZnBC and HA was measured by Inductively Coupled Plasma with Optical Emission Spectrometry (ICP-OES, Spectro Blue, Spectro Analytical Instruments, Germany). Extraction with nitric-perchloric acid digestion was performed for HA and pyrolysis followed by nitric acid (HNO_3, ~65%) and hydrogen peroxide (H_2O_2, ~35%) digestion for BC and ZnBC (Enders et al., 2012). Total, water-soluble (water-P), and neutral ammonium citrate soluble P plus water (NAC + H_2O–P) digestions were performed for MAP fertilizers as described by MAPA - Ministério da Agricultura, and detailed by presenting values of 22.6%, 19.4% and 18.7% of P, respectively. Elemental analysis for C, H and N was performed using an elemental analyzer (model Vario TOC cube, Elementar, Germany).

The phosphorus adsorption capacity of BC and ZnBC was also evaluated by P-remaining (P-rem) test by adding 60 mg L^{-1} of P by KH_2PO_4 solution. Lower P-rem values indicate greater sorption of the material. In addition, electrical conductivity (EC) and pH were measured in an S70 Seven Multi from Mettler Toledo Columbus OH and performed considering the ratio (w/v) of 1:20, after intermittent shaking (90 rpm) for 1.5 h (Zhao et al., 2013).

The specific surface area (SSA) and porous volume (PV) of ZnBC were determined by adsorption of N_2 at 77 K (Quantachrome, model NOVA 2200e). The samples analyzed were prepared according to ASTM D1557 (2007). The BET model (Brunauer et al., 1938) was used to determine the specific surface area (SSA) (P/P_0 between 0.05 and 0.25)

and the PV was estimated by the BJH model (Barrett et al., 1951) in the range 0.99–0.60 P/P_0 through the desorption isotherm. The data were processed using NOVA Win software.

A qualitative investigation of HA and ZnBC functional groups was carried out by Fourier Transform Infrared Spectroscopy with Attenuated Total Reflectance (FTIR-ATR) (Jasco spectrometer, model FT/IR-4100), spectra were collected in the wave number range of 4000 to 500 cm^{-1} with a resolution of 4 cm^{-1} and 256 scans. Both BC, MAPZnBC and MAPHA were evaluated on the basis of their morphology by scanning electron microscopy (SEM) (Jeol, model JSM 6010-LA), using images generated by the LEO 1430 VP. For this purpose, the granules were cut into a cross-sectional shape as can be seen (Fig. 1). The technique of Energy-dispersive X-ray Spectroscopy (EDS) was carried out using a silicon drift detector.

The characterization of the soils after liming is presented in the supplementary material. Physicochemical analyses (Table S1) and X-ray diffraction analysis (XRD) were performed. Mineralogical characterization was performed using a Shimadzu XRD-6000 diffractometer, with a graphite crystal monochromator to select Co-Kα1 radiation (λ = 1.7889 Å) and a step width of 0.02°/s, with 2θ angle between 4° and 70° (Fig. S3).

2.4. Biochar sorption and desorption kinetics

The kinetic study of P was carried out in a continuous flow system as described by Fernández-Calviño et al. (2010). The system consists of solution reservoirs, a piston pump (HPLC – Thermo Scientific, Ultimate 3000), an acrylic reactor (internal volume of 17 mL) mounted on a magnetic stirrer (400 rpm), and an automatic fraction collector (Gilson, FC 203B fraction collector) (Strawn and Sparks, 2000). For each assessment, 0.75 g of BC and ZnBC were added to the reactor. The background solution of 10 μmol L^{-1} KCl in ultrapure water was used to fill the reactor volume and a 10 mm diameter filter paper was used to retain the biochar in the reactor. For the sorption kinetic experiment, 500 μmol L^{-1} KH_2PO_4 and 10 μm L^{-1} KCl in ultrapure water were used. After 250 min, the flow was reversed for desorption and then10 μmol L^{-1} KCl in ultrapure water was used to simulate the ionic strength of the soil solution during desorption. Both the adsorption/desorption solutions were adjusted to pH 6 and the solution flow was kept constant (1 mL min^{-1}) during both evaluations. The sorption/desorption experiments were evaluated in duplicate with the addition of a blank control (without BC) in which the sorption-desorption experiments were performed in the same way. The P contained in the solution leaving the reactor was measured by molecular absorption spectrometry (Braga and Defelipo, 1974). The kinetic curves were obtained through averaging the data for each type of biochar (BC and ZnBC). Sorption (Equation (1)) and desorption (Equation (2)) were calculated according to Fernández-Calviño et al. (2010):

$$q(i) = \left\{ \sum_{j=1}^{i} \left[\frac{(P1(j) - P2(j))\Delta tj}{Ve} \right] + [P1\ (i+1) - P2(i+1)] \right\} \frac{Ve}{m} \quad (1)$$

$$q(i) = \left\{ \sum_{j=1}^{i} \left[\frac{(P2(j) - P1(j))\Delta tj}{Ve} \right] + [P2\ (i+1) - P1(i+1)] \right\} \frac{Ve}{m} \quad (2)$$

being q(i) = adsorption or desorption (mg g^{-1}) accumulated in $i\Delta t$ time (min); P1 (i) and P2 (i) = P concentration in each aliquot in the absence and presence of BC or ZnBC (mg L^{-1}), respectively; J = flow rate (L min^{-1}); Ve = the effective volume of the solution reactor (L); and m = mass of BC or ZnBC (g).

To describe the adsorption and desorption capacity a pseudo-first-order model (Lagergren, 1898) was used and can be represented:

$$\frac{dq_{ads}}{dt} = k_{ads}(q_{max} - q_{ads}) \quad (3)$$

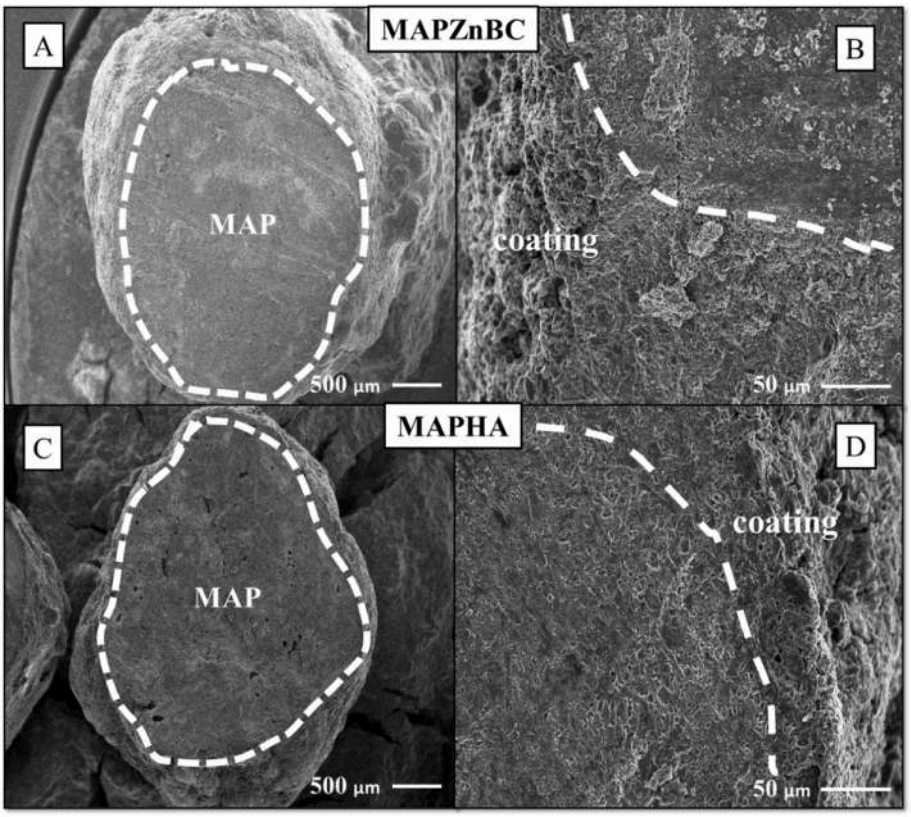

Fig. 1. SEM images of granule surfaces of monoammonium phosphate (MAP) coated with humic acid at 1.0 wt% (MAPHA) or with biochar treated with $ZnCl_2$ at 1.0 wt% (MAPZnBC). (A) cross-section of MAPZnBC (magnification of 27×), (B) cross-section (400×), (C) cross-section of MAPHA (27×), (D) cross-section (400×).

$$\frac{dq_{des}}{dt} des(q_{max} - q_{des}) \quad (4)$$

in which q_{ads} (mg g^{-1}) is the P adsorbed at time t, q_{des} (mg g^{-1}) is the P desorbed at time t, q_{max} is the maximum concentration of P adsorbed or desorbed at equilibrium (mg g^{-1}), k_{ads} (L min^{-1}) and k_{des} (L min^{-1}) are the adsorption and desorption rate constant, respectively. Integration of Equations (3) and (4) with the conditions $t = 0$ to $t = t$, $q_{ads} = 0$ to $q_{ads} = q_{ads}$ and $q_{ades} = 0$ to $q_{des} = q_{des}$:

$$q_{ads} \; or \; q_{des} = q_{max} \left(1 - e^{kt}\right) \quad (5)$$

2.5. P-diffusivity test

A Petri dish experiment was carried out to assess P diffusivity in the fertosphere region. The soils used were two Oxisols (USDA, 2014); a clay Oxisol from Viçosa, Minas Gerais State, Brazil (20°45′37″S and 42°52′04″W, 648 m altitude) and a sandy-loam Oxisol from Três Marias, Minas Gerais State, Brazil (18° 12′ 18″S, 45° 13′ 57″O, 569 m altitude) (Table 1). Soils were collected from the top layer (5–20 cm), air-dried and sieved (<4 mm). Subsamples from each soil were used for chemical, particle-size and mineralogical (XRD) analyses (Table 1). Soil acidity was corrected with a mixture of $CaCO_3$ (0.75 g kg^{-1}) and $MgCO_3$ (0.25 g kg^{-1}) at Ca: Mg molar ratio 3:1.

The treatments were developed by coating MAP with ZnBC or the HA at three coating ratios (0.5, 1.0 and 2.0 wt%) establishing the treatments MAPZnBC or MAPHA with the different coating ratios. A Petri dish without any fertilizer and a MAP without any coating were used as additional treatments. The experiment was carried out in a completely randomized design, with four replications.

To carry out the test, 55 cm^3 of each air-dried soil (clay Oxisol and sandy-loam Oxisol) were placed in Petri dishes (850 × 10 mm), to ensure a flat soil surface. A single granule of each treatment (32 ± 0.02 mg) was placed at a depth of 0.3 cm in the centre of the Petri dish and the soil moisture was increased to 80% of the soil field capacity and kept constant during the incubation. The Petri dishes were then sealed with parafilm to minimize water loss and incubated at 25 °C. All replicates showed similar visual results, therefore only one replicate is shown (Fig. 4).

The P-diffusivity was assessed after 1 and 20 days of incubation using filter paper indicators placed on wet soil surfaces, which turned green when in contact with the soil area where P-diffusivity was present, as detailed by Degryse and McLaughlin (2014). After this process, the filter papers were dried and the green area was measured from scanned images and processed using image software (GNU Image Manipulation Program, v. 2.6.11). The effective radius of diffusion (ERD) was calculated using equation (6), where Ap (mm^2) is the green area coloured by Fe–P species.

$$EDR\ (mm) = \sqrt{Ap/\pi} \quad (6)$$

Table 1
Total contents of chemical elements and physicochemical features of BC, ZnBC and HA (mean value ± standard deviation).

Feature	BC	ZnBC	HA
C (%)	84.3 ± 0.8	57.9 ± 1.2	36.0 ± 0.6
H (%)	3.30 ± 0.5	1.70 ± 0.7	3.41 ± 0.5
N (%)	0.22 ± 0.04	0.31 ± 0.06	1.11 ± 0.05
pH_{H2O}	7.65 ± 0.7	6.12 ± 0.2	9.84 ± 0.1
EC (dS m^{-1})	1.51 ± 0.7	15.6 ± 0.4	–
P_{rem} (mg L^{-1})[e]	50.4 ± 1.2	0.06 ± 0.8	–
P (g kg^{-1})	1.33 ± 0.2	1.13 ± 0.1	1.44 ± 0.38
K (g kg^{-1})	2.92 ± 0.4	1.44 ± 0.1	67.4 ± 5.11
Ca (g kg^{-1})	1.52 ± 0.3	0.00 ± 0.0	10.5 ± 0.21
S (g kg^{-1})	0.91 ± 0.1	0.90 ± 0.1	4.40 ± 0.35
Mg (g kg^{-1})	0.73 ± 0.1	0.51 ± 0.2	1.41 ± 0.23
Zn (g kg^{-1})	0.95 ± 0.0	49.6 ± 3.3	0.00 ± 0.02
Fe (g kg^{-1})	2.41 ± 0.2	5.70 ± 0.5	4.12 ± 0.48
Al (g kg^{-1})	0.72 ± 0.02	2.72 ± 0.2	10.3 ± 0.37
Si (g kg^{-1})	0.63 ± 0.0	0.63 ± 0.0	0.00 ± 0.0
Ni (g kg^{-1})	0.30 ± 0.05	1.00 ± 0.0	0.00 ± 0.0

Note: elemental analysis, n = 3 and P_{rem}, n = 3.
[a] Electric conductivity (n = 3).

2.6. P-soil release

A kinetic study was carried out to evaluate the effect of the coating on P-release in the fertosphere environment. It was carried out in a continuous stirred-flow system as described by Benício et al. (2017), using Petri dishes and the same clay Oxisol used previously. As there was no significant difference between the coating ratios (0.5, 1.0 and 2.0 wt %) in the diffusion test, MAPZnBC (1.0 wt%) and MAPHA (1.0 wt%) were selected for this and subsequent tests. After 30 d of incubation at 25 °C and controlled humidity (80% of the soil field capacity), soil samples were collected using a ring with 1.25 cm in diameter and 1.0 cm high (~1.23 cm^3), taking as reference the centre of the Petri dishes where the fertilizer granule was applied. The soil samples were subjected to P-desorption using a continuous stirred-flow system (1 mL min^{-1}) and constantly stirred (100 rpm) by a magnetic stirrer using a solution of 10 μmol L^{-1} of KCl with deionized water at pH 6 (simulating the soil solution) and controlled environment at 20 °C. For all kinetic runs, a mass of 0.75 g of soil was used and added to the reactor (14 mL). The soil sample was retained in the chamber by a 0.45 μm cellulose membrane placed in the upper part of the chamber. When the system was switched on, the desorption solution passed through the chamber and thus through the sample. The effluent was collected every 2 min for 100 min and desorption runs were performed in triplicate. The phosphorus content of the effluent was measured by molecular absorption spectrometry (Braga and Defelipo, 1974). The cumulative P-soil release was then calculated as the sum of the desorption over time used in the test. The percentage of P recovery in the fertosphere was calculated based on the initial mass of P added via MAP granules minus the total P desorbed from the control treatment, without the addition of fertilizers.

2.7. Pot experiment

To compare the agronomic performance of MAP in contrast with MAPZnBC and MAPHA materials, maize (*Zea mays* L.) was grown followed by soybean (*Glycine* max L.). The fertilizers MAPZnBC and MAPHA at 1.0 wt% were selected based on diffusivity results, which showed that both ZnBC and HA coatings altered MAP diffusivity independently of the coating ratio. The experimental design adopted was complete randomized-block in a double factorial scheme plus an additional treatment [(3 × 4) + 1], consisting of three P sources (MAP, MAPZnBC 1% and MAPHA 1%), four P rates (100, 200, 300 and 400 mg dm^{-3} P), and an additional treatment (no P application). The soil used was the clay Oxisols (Viçosa, Minas Gerais State, Brazil), which was collected, pH adjusted and characterized (Table 1).

Phosphorus rates were applied locally in the centre of the pot, using 30% of the soil pot volume to mix the granules. For the first crop (maize), three seeds were sown in each pot and thinned to two seedlings after 3 days. A multi-element solution containing N, K, S, B, Zn, Cu, Mn and Mo was added at 10, 20 and 30 days after sowing, providing, 200 mg dm^{-3} N, 150 mg dm^{-3} K, 50 mg dm^{-3} S, 1.21 mg dm^{-3} B, 4.5 mg dm^{-3} Zn, 1.3 mg dm^{-3} Cu, 5.4 mg dm^{-3} Mn and 0.15 mg dm^{-3} Mo to ensure adequate fertility conditions for plant growth in greenhouse experiments (Novais et al., 1991). Soil moisture was checked daily to maintain at ~80% of the water field capacity. After 45 d of growth, maize shoots were harvested at the soil surface (6 cm above ground). After maize harvest, soybean inoculated with *Bradyrhizobium* sp. was sown in undisturbed soil pots at 2 cm of depth. After seedling emergence, only two plants were maintained in each pot. A solution containing Zn, Cu, Mn and Mo was added at 10, 20 and 30 d after sowing, providing 4.5, 1.3, 5.4 and 0.15 mg dm^{-3}, respectively. After 48 days,

soybean shoots were harvested by cutting the stems at the soil surface. Plant tissues were oven-dried at 65 °C for 72 h (to constant weight), weighed and ground for chemical analysis. Plant tissues were then subjected to nitric-perchloric acid digestion (EMBRAPA, 2000) and P content was quantified by ICP-OES (Agilent, Series AA Model 240 FS). Phosphorus use efficiency (P_{UE}) is defined as the shoot dry matter per unit P uptake (g SDM mg^{-1} P) (Rose and Wissuwa, 2012). Phosphorus uptake in shoots (P_{upt}) was calculated by multiplying SDM by P content, while P_{UE} was calculated as described by Equation (7):

$$P_{UE}(\%) = \frac{\left(P_{upttoal} - P_{uptcontrol}\right)}{Pdose} x\ 100 \quad (7)$$

in which $P_{upttotal}$ is the P uptake (mg pot^{-1}) in the plant tissue, $P_{uptcontrol}$ is the P uptake (mg pot^{-1}) in the plant tissue in the control treatment (without P addition) and P_{dose} is the amount of P applied as phosphate fertilizer (mg kg^{-1}). For the second cropping cycle, the P uptake by the first cycle was also subtracted.

2.8. Statistical analyses

The data were subjected to analysis of variance (two-way ANOVA, α = 5%) using R software (R Core Team, 2022) and employing the ExpDes package (Ferreira et al., 2014). The P diffusivity means for different coatings at the same time and coating ratios in different soils were compared using the Tukey test (α = 5%). In the pot experiment, the regression models (Regazzi, 1999) describing SDM, P uptake in maize and soybean in response to different P sources and rates were subjected to an identity test ($p < 0.05$).

3. Results

3.1. Characterization studies

The SEM images of ZnBC and BC in the Supplementary Data (Fig. S1) showed a marked difference in the shape of individual particles, pores, voids and cracks on the surface of ZnBC compared to BC. The SEM images of MAPZnBC and MAPHA also show the composition of the fertilizers produced by the coating technique. There are two phases, the core and the coating (Fig. 1). SEM images of MAPZnBC and MAPHA showed that both ZnBC and HA as coatings produced remarkable amounts of pores and voids on the surfaces. In addition, EDS analysis was carried out on BC and ZnBC and showed that Zn, C and O (Fig. S1) are homogeneously distributed throughout the material.

The FTIR spectrum of ZnBC (Fig. S2) showed characteristic peaks of carbon compounds. The peak at 1560 cm^{-1} represented stretching vibration of aromatic rings (C=C) (Keiluweit et al., 2010; Song et al., 2020). In addition, the band at 1157 cm^{-1} is related to C–O stretching (Liou and Wu, 2009), and a broad band at 3400 cm^{-1} related to adsorbed water was observed, indicating stretching of O–H groups associated with phenol or alcohol and water functional groups (Keiluweit et al., 2010). Moreover, the small band at 2929 cm^{-1} is assigned to C–H stretching vibrations of aliphatic compounds. HA showed an absorption band in the range between 3400 and 3200 cm^{-1}, which is typical for O–H stretching vibrations (Pookmanee et al., 2016). The absorption bands around 1200–1100 are due to the presence of the C–O group. The peaks at ~1620-1420 cm^{-1} have been assigned to aromatic ring-like C=C stretching mode in polyaromatics (Sarlaki et al., 2021).

Wood-based biochar tends to contain more C and less plant nutrients in its composition when compared to other raw materials such as manure (Ippolito et al., 2020). However, impregnation with $ZnCl_2$ resulted in an increase in total zinc content of 49.59 g kg^{-1} (Table 1). Zinc impregnation caused a decrease in C and H contents of 28% and 1.5%, respectively. The C content decreased on the activated material (ZnBC) due to the release of CO and CO_2 (Liou and Wu, 2009). P-rem showed that BC has low effectiveness in P adsorption, unlike activated ZnBC, which adsorbs almost all the added phosphorus (Table 1). On the other hand, HA showed expressive contents of macronutrients when compared to BC and ZnBC, with emphasis on K and Ca.

ZnBC and BC isotherms (Fig. 2) and the physicochemical properties (Table S1) show how the co-pyrolysis of eucalyptus biomass with $ZnCl_2$ can influence the formation of biochar as a final product, mainly in terms of desirable properties for an adsorbent material. ZnBC exhibited three times higher specific surface area (939.7 m^2 g^{-1}) than BC. In addition, the total pore volume and the average pore radius were also improved for ZnBC. The isotherm showed by ZnBC and BC (Fig. 2) indicates different patterns of adsorbent materials. According to the International Union of Pure and Applied Chemistry (IUPAC) classification, porous materials should be classified by porosity and gas sorption isotherms. In this sense, the nitrogen adsorption-desorption isotherm of ZnBC is classified as type I, which refers to adsorbents with monolayer adsorption and microporous characteristics (Lowell et al., 2006; Pierotti and Rouquerol, 1985). On the other hand, the BC isotherm pattern should be categorized as type IV, which shows hysteresis between N_2 absorption and desorption. This configuration is characterized by materials with fewer pores and a greater proportion of macropores in the structure (Lowell et al., 2006).

3.2. Sorption and desorption kinetics

Phosphorus sorption and desorption were fast during the kinetic evaluation, especially for ZnBC (Fig. 3). The sorption rate increased between 40 and 80 min and equilibrium was reached within approximately 200 min of the evaluation for both materials. A maximum sorption capacity of 51.8 and 102.8 mg g^{-1} P was reached in 250 min for

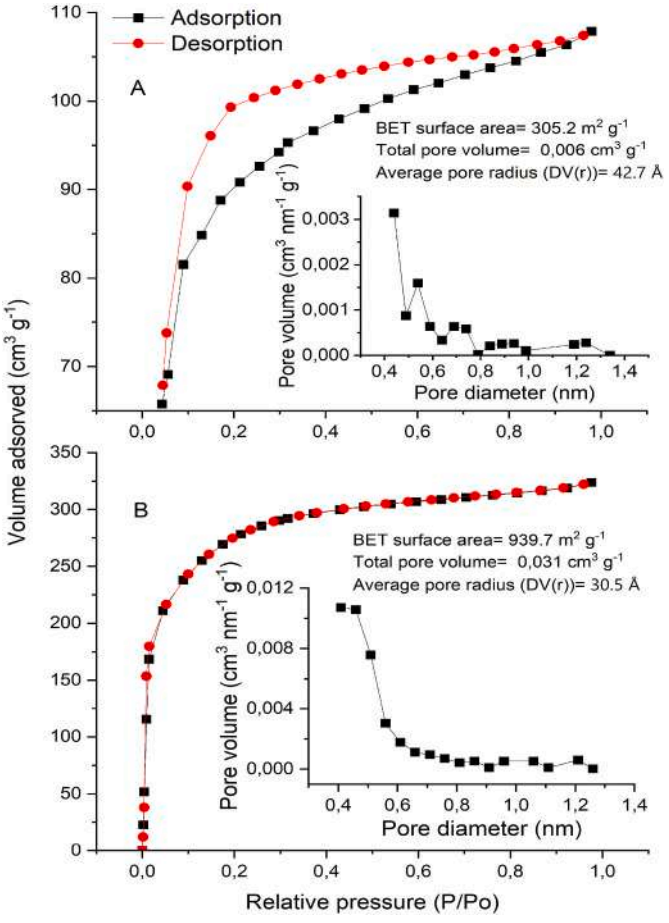

Fig. 2. Nitrogen adsorption-desorption isotherm and pore size distributions of BC (A) and ZnBC (B).

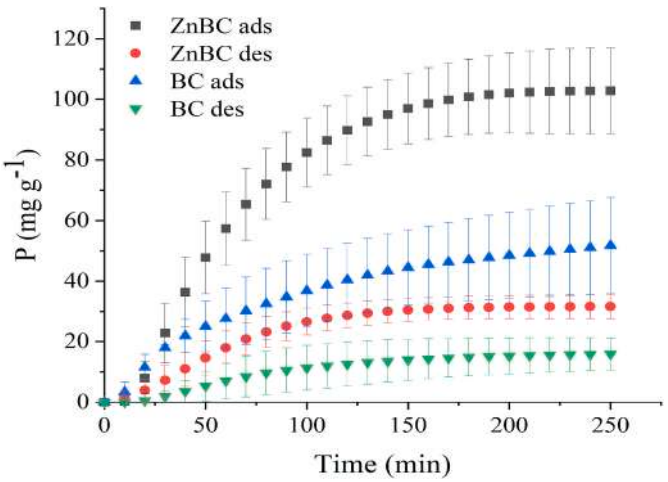

Fig. 3. Cumulative P adsorption (ads) and desorption (des) by biochar (BC) or zinc biochar (ZnBC) in stirred-flow system. Data are presented as mean values of duplicates with bars indicating the standard error of the mean.

BC and ZnBC, respectively. Desorption increased rapidly between 40 and 50 min, reaching values of 15.9 and 31.6 mg g^{-1} P for BC and ZnBC, respectively. With the same desorption rate (~30%), ZnBC showed an almost 2-fold higher phosphate adsorption potential compared to BC. The parameters of adsorption/desorption parameters evaluated by the pseudo-first-order model showed a high correlation of the model applied to the data (Table 2).

3.3. Phosphorus diffusion

The diffusion coefficient is the proportionality between flux and concentration gradient and is an important parameter indicating mobility (Baur, 2007). Both sorption and precipitation responses are influenced by the high concentration around a fertilizer granule, the fertosphere (Bolland and Gilkes, 2017). The environmental and agronomic efficiency of a fertilizer depends heavily on its ability to synchronize nutrient release with plant uptake patterns. The environmental and agronomic efficiency of a fertilizer depends heavily on its ability to synchronize nutrient release with plant uptake patterns. A higher ERD for fertilizers can mean an increase in root access to a particular nutrient. However, for phosphate fertilizers, a higher ERD means an increase in the contact area between the phosphate molecules and the mineral surface, leading to an increased chance of sorption reactions and risk of leaching.

In general, both fertilizer coatings (MAPZnBC and MAPHA) resulted in a decrease in granule diffusivity, especially after day 20 of evaluation in the sand soil (Fig. 4). Diffusion occurred rapidly on day 1 of incubation for all treatments. As expected, the sandy-loam Oxisol had a higher diffusivity than the clay Oxisol over the whole evaluation period. For the clay Oxisol, MAPZnBC decreased diffusivity compared to MAPHA and MAP in the global average for the day 1 evaluation (Fig. 4a) and no difference was observed between the coating ratios (0.5, 1.0 and 2.0 wt %). At day 20, both MAPHA and MAPZnBC decreased the overall ERD compared to MAP and only MAPZnBC (0.5 wt%) increased the ERD compared to the other coating ratios at day 20 of the evaluation (Fig. 4b). In contrast, no differences were observed on sandy-loam Oxisol on day 1 (Fig. 4c). MAPHA and MAPZnBC showed lower global ERD compared to MAP on day 20 (Fig. 4d). Moreover, only MAPHA 0.5% showed a higher ERD compared to MAPHA 1 and 2% (Fig. 4d).

3.4. P-soil release

The accumulated desorption corresponds to the sum of the labile phosphorus values in water obtained at each time point (min) in the fertosphere (Fig. 5a). Both MAPZnBC and MAPHA showed a greater ability to retain P in the readily labile form in the fertosphere region compared to MAP after 30 days of incubation. Furthermore, MAPZnBC and MAP were 20% and 34% more efficient than MAP in the recovery of water-soluble phosphate (Fig. 5b).

3.5. Pot experiment

A Significant increase in SDM by MAPZnBC and P uptake by MAPHA was observed compared to the MAP between each crop cycle and in the sum of both cultivations (Fig. 6 and Table S3). Although there was no difference for P uptake in the first and second crop cycles, a significant difference was observed between MAPZnBC and MAP for SDM (Fig. 6a and b). On the other hand, MAPHA showed a positive difference compared to MAP for P uptake in the first crop cycle and the total P uptake (Fig. 6c and f). When comparing ZnBC and HA as coatings, MAPZnBC showed significant differences for SDM, while MAPHA accumulated uptake after the first cultivation (Fig. 6a and c). In addition, MAPHA showed a positive increase in SDM and P uptake in the second cultivation (Fig. 6b and d). There was also an increase in total P uptake by MAPHA in the sum of the cycles (Fig. 6f) and PUE (Fig. 5c) compared to MAP and MAPZnBC.

4. Discussion

4.1. Sorption and desorption kinetics of biochar

Adsorption/desorption kinetics consist of the rate at which an adsorbent removes a given adsorbate in an aqueous medium (by different mechanisms) (Zhang et al., 2015). Chemical modifications can alter properties of biochar such as surface area, functional groups and adsorption selectivity (Li et al., 2021). The effectiveness of $ZnCl_2$ enrichment during co-pyrolysis to promote phosphate retention can be attributed to several mechanisms such as ligand exchange, physical adsorption, chemical adsorption, co-precipitation or complexation exchange (Luo et al., 2022). Some of these interactions are attributed to the formation of new zinc-rich functional groups and pores on the biochar surface generated during pyrolysis. Zinc-containing substances are also effective and low-cost modification agents for improving pore structure, increasing the surface area, activating functional groups, and forming zinc oxide (ZnO) nanoparticles on biochar (Yan et al., 2020). The increase in physicochemical properties of biochar by Zn is due to the conversion of part of the $ZnCl_2$ into ZnO during pyrolysis, which is involved in increasing the total pore volume and microporous structure on BC (Perondi et al., 2021). In certain cases, the surface area may decrease as the pore volume increases. However, there are cases where both increase. As pore volume increases, the number of pores (where nitrogen is located) can increase, facilitating an increase in BET surface area (Scherdel et al., 2010). A schematic representation of the role of Zn in the ZnBC surface and sorption mechanisms can be found in the supplementary material. (Fig. S4).

The shape of the isotherm can essentially describe the sorption/desorption process and can therefore be used to interpret the nature of the sorption (Inglezakis and Fyrillas, 2017). Among the isotherm types, Fig. 2 shows that ZnBC exhibits an H-type isotherm (high affinity), which is characterized by a sharp vertical part of the initial slope and high interaction between adsorbate and adsorbent (Sahoo and Prelot, 2020). In addition, the isotherm can also be used to interpret sorption and desorption with respect to porous materials. According to the International Union of Pure and Applied Chemistry (IUPAC) classification, a concave shape with respect to the P/P0 axis (Type I) indicates a reversible adsorption mechanism limited to monolayer adsorption (Fig. 2). In this state, the physical mechanism of adsorption predominates, indicating a microporous material (Lowell et al., 2006).

On ZnBC, orthophosphate species ($H_xPO_4^{x-3}$) can react with Zn^{2+} in different ways. The co-precipitation of ZnP species can be favoured by

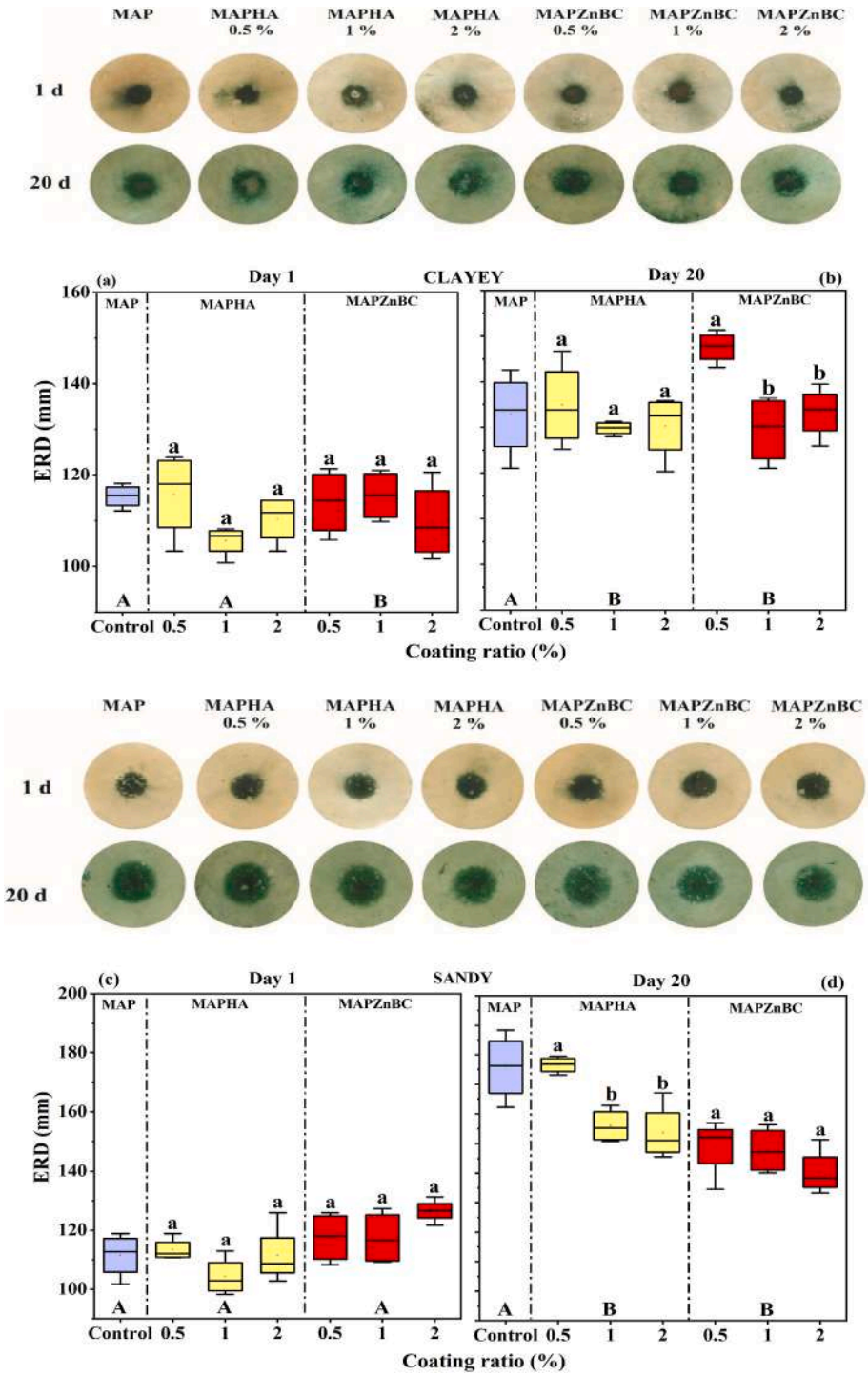

Fig. 4. Visualization of the P diffusion zone at 1 and 20 days after addition of the fertilizer granules and incubation on clay and sand-loam Oxisols by MAPHA and MAPZnBC with coatings ratios of 0.5, 1 and 2 wt % and the control MAP. The dark green zone represents the high-P zone, and it was determined by image processing. Effective radius of diffusion (ERD) of clay (Fig. 4a and b) and sandy-loam Oxisols (Fig. 4c and d) after 1 day and 20 days of incubation, respectively. Note: Columns with the same letter are not statistically different ($p < 0.5$) according to the Tukey test. Capital letters – comparison of different fertilizers at the same time of incubation. Lower case letters – comparison of different coating ratios within each treatment.

Table 2
Parameters of P adsorption and desorption by BC and ZnBC by Largergren model.

Biochars	Adsorption			Desorption		
	q_{max} (mg g^{-1})	k (min^{-1})	R^2	q_{max} (mg g^{-1})	k (min^{-1})	R^2
ZnBC	106	1.16×10^{-2}	0.97[a]	33	1.26×10^{-2}	0.97[a]
BC	53	1.19×10^{-2}	0.97[a]	17	8.0×10^{-3}	0.97[a]

[a] Indicates p value > 0.05.

the increase in porosity when compared to the original BC. In addition, phosphate species are complexed by Zn^{2+}, which has empty d-orbitals and could receive electrons from PO_4^{3-}, increasing phosphate adsorption from solution (Nakarmi et al., 2020). Both physical and chemical adsorption of Zn on the biochar structure allows the formation of cationic bridges more homogeneously on the biochar surface, capable of retaining P with different energetic and reversibility magnitudes. Despite desorption with 10 μm L^{-1} KCl solution, it could be seen that only 25% of the adsorbed P was desorbed due to the strong energy on phosphate interactions and the stability of precipitated and/or complexed species formed (Fig. 3).

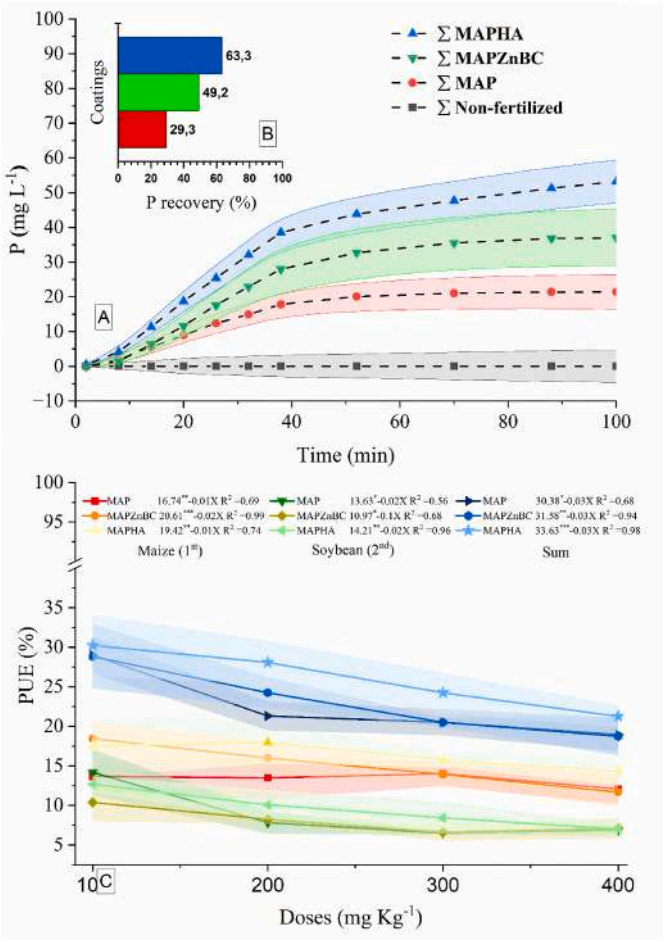

Fig. 5. (A) Cumulative P-soil release by stirred flow system after 30 days incubation in a clay Oxisol soil with MAPHA (1%), MAPZnBC (1%), MAP, and a non-fertilized control (width of bars represents standard deviation, n = 3) and (B) P recovery rate from the fertosphere of each treatment in relation to the initial P added; (C) Phosphorus use efficiency (PUE) per dose by MAPHA (1%), MAPZnBC (1%) and MAP (width of bars represents standard deviation, n = 3).

4.2. Diffusivity

It has been hypothesized that ZnBC would reduce phosphate diffusivity, due to the high adsorption capacity of the ZnBC for phosphate (Bacelo et al., 2020). On the other hand, HA coating has the role of acting on the soil surface minerals in the fertosphere as a soil conditioner, acting on the interaction between P and Al and Fe (oxy)hydroxides through competition and affinity for binding sites (Fu et al., 2013; Gimsing et al., 2004; Wang et al., 2016). In this case, the presence of HA was hypothesized to increase the diffusion potential of the granule by decreasing specific adsorption of phosphate. However, the current study demonstrated that both materials decreased phosphate released by these actions (Fig. 4).

In terms of controlled release, although ZnBC is a highly resistant structure, the coating surface should affect its ability to protect MAP from soaking. According to Kinney et al. (2012), the 3000-2800 cm^{-1} peak area (alkyl peak) correlates with hydrophobic properties. However, there is a tendency for these groups to disappear when pyrolysis is performed at temperatures above 400 °C (Xia et al., 2016). Furthermore, as observed through the SEM (Fig. 1), the ZnBC coating presents an uneven surface with holes and cracks, which does not prevent the solubilization of the granules. Moreover, HA does not exhibit the characteristics of a control-release fertilizer, as observed in other materials (Volf and Rosolem, 2021). HA is highly soluble at pH values above 2 (Mobed et al., 2000), therefore its rapid dissolution as a coating material is highly expected at pH around 6.0 and high soil moisture (~80%) as in the present study. From the aspect of increasing P diffusivity, HA might be able to reduce phosphate adsorption by the surface of (oxy)hydroxides and due to HA-metal complexation interaction. However, these functions were not shown to be able to increase P diffusivity even on soils with contrasting textures (Fig. 4).

Compared to MAP, ZnBC and HA coatings were able to reduce diffusivity (Fig. 4), although they did not reduce the solubility of the fertilizer granules. However, reduced diffusivity cannot necessarily be interpreted as reduced P availability. McBeath et al. (2012) evaluated P and Zn availability of fertilizers applied to dry and wet soils at 80% of field capacity. The authors verified that P diffusivity decreased, but there were no changes in plant available P levels. Also, Lustosa Filho et al. (2019) impregnated poultry litter with TSP and H_3PO_4 with and without MgO aiming to produce biochar-based fertilizers (BBFs). They verified that P diffusion was slower and more gradual for the PLB-H_3PO_4–MgO and PLB-TSP-MgO treatments and proceeded more gradually as compared to conventional fertilizer (triple superphosphate – TSP). However, the BBFs were able to supply P to the plants similarly to TSP.

4.3. P-soil release

A proposed strategy to improve PUE is the development of controlled-release, chemically modified, slow-release or even synergistic P fertilizers to decelerate specific P-soil bonds in addition to acting in synchrony with plant requirements (Vejan et al., 2021). As discussed by Glaser and Lehr (2019), the addition of pristine biochar significantly increased P availability in agricultural soils, regardless of the raw materials used to produce the biochar. However, a significant increase in P availability in agricultural soils was only achieved with biochar applications above 10 Mg ha^{-1}. Considering the increase in P availability in the release assay (Fig. 5a and b), it should be noted that biochar engineering, such as activation with $ZnCl_2$, helps to increase the efficiency of this material (Chhimwal et al., 2022), even when used in small quantities as a coating technology.

Both ZnBC and HA not only separate MAP from direct contact with the soil, but also prevent P from being fixed by the soil through sorption, complexation and precipitation (Roberts and Johnston, 2015). The ZnBC coating acts as a matrix for phosphorus sorption/desorption between the granule and the fertosphere. On the other hand, HA performs preferentially as a competition/complexing agent.

The difference observed between MAPZnBC (1%) and MAP is due to the fact that ZnBC is a material with higher adsorption capacity due to its SSA and PV in relation to BC (Table 1). Conversely, it can be noticed that ZnBC is also able to desorb P. The adsorption and desorption potentials indicate the usability of the sorbent (Kołodyńska et al., 2017) by comparing the desorption kinetics of ZnBC phosphorus (Fig. 3) with the cumulative desorption on the fertosphere (Fig. 5a and b). This property is essential for materials that need to recover and release elements and have a buffering effect on the environment.

HA is not a substance with intrinsic adsorption properties, although it can alter soil exchange and adsorption capacity (Zavaschi et al., 2020). MAPHA showed the highest P recovery rate in the fertosphere, even compared to MAPZnBC (Fig. 5a and b). Since HA is an important component of humic substances (Antelo et al., 2007), the phosphate desorption and recovery rate observed in this work are consistent with data of Wang et al. (2016). They observed a positive effect using HA in reducing phosphate ($H_2PO_4^-$, $HPO4^{2}$) adsorption on (oxy)hydroxides. Such a decrease in phosphate adsorption on the surface of iron (oxy) hydroxides such as hematite and goethite occurs due to competition for specific binding sites on their surface. Moreover, the application of HA in soil leads to a modification of the surface interaction by changing the charges through the development of a repulsive negative electric potential on the mineral surface (Chen et al., 2021). On the other hand

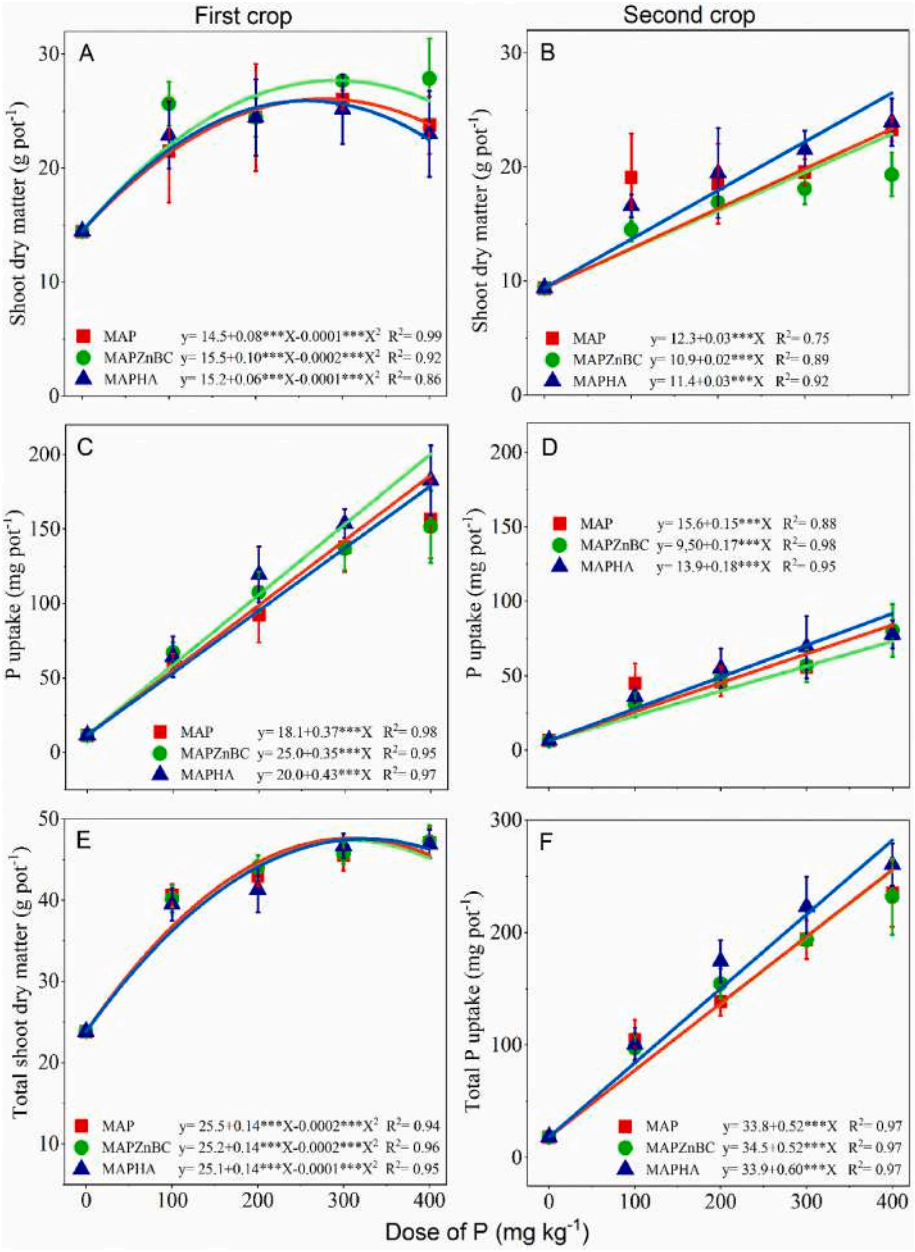

Fig. 6. Shoot dry matter, P uptake, total dry matter and total P uptake in the first crop (maize) and second crop (soybean) as a function of P rates and different additives as MAP (control with no coating), MAPHA (1%) and MAPZnBC (1%).

(Borggaard et al., 2005), observed little impact of humic amendments at concentrations comparable to natural levels on the phosphate adsorbed by synthetic aluminium oxide, ferrihydrite and goethite. However, recent research shows positive effects on nutrient storage capacity and inhibition of P binding to the mineral surface by HA as a coating (Chen et al., 2021). These results show that the concentration, type of organic source, and the evaluation method can influence the observations of the humic substances on P soil availability (Sims et al., 2005).

4.4. Pot experiment

The ANOVA results show that ZnBC and HA as coating (wt%) and applied P doses had a significant effect on crop parameters such as SDM, P uptake and P recovery rate ($P < 0.05$) (Table S2). Regardless of the coating type or crop cycle, increasing the P dose did not show an additive effect of ZnBC and HA coatings on the observed parameters, even at the highest P doses (Fig. 6). Furthermore, in situations of high phosphate concentration, highly weathered soils and clay content, the P recovery rate decreases at the expense of increasing non-labile P fractions (Vance et al., 2003). In the first crop cycle, ZnBC as a P buffer matrix between the granule-soil-root allowed an increase in SDM compared to MAP (Fig. 6a). However, no difference in accumulated P uptake was observed between MAPZnBC and MAP, demonstrating that another effect of ZnBC interacts with maize growth. Studies have shown that ion exchange capacity, water retention and improvement of the soil microfauna community can be associated with the use of BC on soils (Ali et al., 2020). Although P-soil release revealed that the clay Oxisol incubated with MAPZnBC had ~20% higher labile P as compared to the MAP (Fig. 5a), this recovery rate may not be expressed in P use and efficiency in crops (Fig. 5c). A meta-analysis carried out by Tesfaye et al. (2021) showed that BC application to soil can alter P availability and plant uptake, increasing them by an average of 55% and 65% respectively. As ZnBC has the characteristics to act as a matrix for P adsorption due to SSA and pore volume as discussed previously, it is necessary to

carry out long-term studies on biochar-based fertilizers and PUE.

Meanwhile, MAPHA increased P uptake in the first cultivation, resulting in a higher total P uptake in the sum of the two cycles (Fig. 6c and f), as well as higher SDM in the second crop (Fig. 6b) and PUE (Fig. 5c). The use of HA as an additive in phosphate fertilizers may increase the rate of P recovery, probably due to its interaction with the soil and P kinetics (Morales et al., 2013) in the fertosphere. These results are also consistent with the data observed in the stirred flow desorption experiment (Fig. 5a and b), where MAPHA showed high P availability compared to MAP and MAPZnBC. Studies have also shown that the application of HA can improve the efficiency of high soluble fertilizers and PUE (Izhar Shafi et al., 2020; Xu et al., 2021). In addition, plant physiological effects are also observed through the action of HA in fertilizers. Chen et al. (2021) observed that application of coated diammonium phosphate and HA altered the exudation profile of maize roots, increasing acid phosphatase activity, ATP synthase activity and cytokinin content. Such effects of applying HA application are difficult to disentangle from its effect on soil P availability for plant growth.

5. Conclusions

The results confirmed the effectiveness of ZnBC and HA as a coating for P availability of a highly soluble phosphate fertilizer in the fertosphere. The use of $ZnCl_2$ as a catalyst in the pyrolysis process has increased the surface area and functional groups of ZnBC, as well as its pore volume, allowing this high capacity to remove P from solution. Both MAPZnBC and MAPHA coatings reduced the diffusivity of the phosphate fertilizer while increasing the water-soluble P in the fertosphere after soil incubation. Evaluation at the fertosphere scale shows that ZnBC can act as a buffer matrix, retaining some of the P released during granule dissolution. Although MAPZnBC improved P availability from MAP, no increase in P uptake was observed. On the other hand, MAPHA decreased P sorption in the fertosphere, resulting in the highest P recovery rate and PUE compared to MAPZnBC and MAP. The HA-metal interaction, which competes with P for binding sites on soil (oxy)hydroxides appears to be the most promising mechanism for improving PUE. The use of carbon-based coatings has had a major effect on P availability in the fertosphere, but as the intrinsic properties of the fertilizer and soil dominate over the coating layer, the long-term residual effects of the coating need to be assessed in the future.

Credit author statement

Maurício Cunha Almeida Leite: Conceptualization, Formal analysis, Investigation, Writing - original draft; **Fabiane Carvalho Ballotin**: Formal analysis, Writing - review & editing; **José Ferreira Lustosa Filho**: Writing and review; **Wedisson Oliveira Santos**: Conceptualization, Writing and review; **Patrícia Cardoso Matias**: Formal analyses and review; **Denison Pogorzelski**: Conceptualization and review; **Leonardus Vergutz**: Conceptualization and review; **Edson Marcio Mattiello**: Funding acquisition, Conceptualization, Supervision.

Declaration of competing interest

The authors declare that they have no known competing financial interests or personal relationships that could have appeared to influence the work reported in this paper.

Data availability

Data will be made available on request.

Acknowledgment

The authors gratefully acknowledge funding received from Conselho Nacional de Desenvolvimento Científico e Tecnológico (CNPq) and Fertilizantes Heringer.

Appendix A. Supplementary data

Supplementary data to this article can be found online at https://doi.org/10.1016/j.envres.2023.115927.

References

Ali, M.A., Ajaz, M.M., Rizwan, M., Qayyum, M.F., Arshad, M., Hussain, S., Ahmad, N., Qureshi, M.A., 2020. Effect of biochar and phosphate solubilizing bacteria on growth and phosphorus uptake by maize in an Aridisol. Arabian J. Geosci. 13 https://doi.org/10.1007/s12517-020-05326-6.

Altintig, E., Kirkil, S., 2016. Preparation and properties of Ag-coated activated carbon nanocomposites produced from wild chestnut shell by ZnCl2 activation. J. Taiwan Inst. Chem. Eng. 63, 180–188. https://doi.org/10.1016/j.jtice.2016.02.032.

Ampong, K., Thilakaranthna, M.S., Gorim, L.Y., 2022. Understanding the role of humic acids on crop performance and soil health. Front. Agron. 4 https://doi.org/10.3389/fagro.2022.848621.

Antelo, J., Arce, F., Avena, M., Fiol, S., López, R., Macías, F., 2007. Adsorption of a soil humic acid at the surface of goethite and its competitive interaction with phosphate. Geoderma 138, 12–19. https://doi.org/10.1016/j.geoderma.2006.10.011.

ASTM D1557, 2007. Standard Test Methods for Laboratory compaction characteristics of soil Using Modified Effort. ASTM International, 56,000ftlbf/ft3 (2,700 kN-m/m3.

Bacelo, H., Pintor, A.M.A., Santos, S.C.R., Boaventura, R.A.R., Botelho, C.M.S., 2020. Performance and prospects of different adsorbents for phosphorus uptake and recovery from water. Chem. Eng. J. 381, 122566 https://doi.org/10.1016/j.cej.2019.122566.

Barrett, E.P., Joyner, L.G., Halenda, P.P., 1951. The determination of pore volume and area distributions in porous substances. I. Computations from nitrogen isotherms. J. Am. Chem. Soc. 73, 373–380.

Baur, J.E., 2007. 19 – diffusion coefficients. In: Zoski, C.G. (Ed.), Handbook of Electrochemistry. Elsevier, Amsterdam, pp. 829–848. https://doi.org/10.1016/B978-044451958-0.50036-7.

Benício, L.P.F., Constantino, V.R.L., Pinto, F.G., Vergütz, L., Tronto, J., Da Costa, L.M., 2017. Layered double hydroxides: new technology in phosphate fertilizers based on nanostructured materials. ACS Sustain. Chem. Eng. 5, 399–409. https://doi.org/10.1021/acssuschemeng.6b01784.

Bolland, M.D.A., Gilkes, R.J., 2017. The chemistry and agronomic effectiveness of phosphate fertilizers. In: Nutrient Use in Crop Production. CRC Press, pp. 139–163.

Borggaard, O.K., Raben-Lange, B., Gimsing, A.L., Strobel, B.W., 2005. Influence of humic substances on phosphate adsorption by aluminium and iron oxides. Geoderma 127, 270–279. https://doi.org/10.1016/j.geoderma.2004.12.011.

Braga, J.M., Defelipo, B.V., 1974. Determinação espectrofotométrica de fósforo em extratos de solos e plantas. Rev. Ceres 21, 73–85.

Brunauer, S., Emmett, P.H., Teller, E., 1938. Adsorption of gases in multimolecular layers. J. Am. Chem. Soc. 60, 309–319.

Chen, Q., Qu, Z., Li, Z., Zhang, Z., Ma, G., Liu, Z., Wang, Y., Wu, L., Fang, F., Wei, Z., 2021. Coated diammonium phosphate combined with humic acid improves soil phosphorus availability and photosynthesis and the yield of maize. Front. Plant Sci. 12.

Chhimwal, M., Pandey, D., Srivastava, R.K., 2022. Pristine biochar and engineered biochar: differences and application. In: Engineered Biochar: Fundamentals, Preparation, Characterization and Applications. Springer, pp. 3–19.

Dai, Z., Xiong, X., Zhu, H., Xu, H., Leng, P., Li, J., Tang, C., Xu, J., 2021. Association of biochar properties with changes in soil bacterial, fungal and fauna communities and nutrient cycling processes. Biochar 3, 239–254. https://doi.org/10.1007/s42773-021-00099-x.

Degryse, F., McLaughlin, M.J., 2014. Phosphorus diffusion from fertilizer: visualization, chemical measurements, and modeling. Soil Sci. Soc. Am. J. 78, 832. https://doi.org/10.2136/sssaj2013.07.0293.

Della Lucia, M.C., Bertoldo, G., Broccanello, C., Maretto, L., Ravi, S., Marinello, F., Sartori, L., Marsilio, G., Baglieri, A., Romano, A., Colombo, M., Magro, F., Campagna, G., Concheri, G., Squartini, A., Stevanato, P., 2021. Novel effects of leonardite-based applications on sugar beet. Front. Plant Sci. 12, 1–10. https://doi.org/10.3389/fpls.2021.646025.

El-Naggar, A., Lee, S.S., Awad, Y.M., Yang, X., Ryu, C., Rizwan, M., Rinklebe, J., Tsang, D.C.W., Ok, Y.S., 2018. Influence of soil properties and feedstocks on biochar potential for carbon mineralization and improvement of infertile soils. Geoderma 332, 100–108. https://doi.org/10.1016/j.geoderma.2018.06.017.

EMBRAPA, 2000. Métodos de Análises de Tecidos vegetais utilizados na embrapa solos. Embrapa solos 41.

Enders, A., Hanley, K., Whitman, T., Joseph, S., Lehmann, J., 2012. Bioresource Technology Characterization of biochars to evaluate recalcitrance and agronomic performance. Bioresour. Technol. 114, 644–653. https://doi.org/10.1016/j.biortech.2012.03.022.

FAO, 2018. The Future of Food and Agriculture: Alternative Pathways to 2050. Food Agric. Organ. United Nations Rome.

Fernández-Calviño, D., Pérez-Novo, C., Bermúdez-Couso, A., López-Periago, E., Arias-Estévez, M., 2010. Batch and stirred flow reactor experiments on Zn sorption in acid soils. Cu competition. Geoderma 159, 417–424. https://doi.org/10.1016/j.geoderma.2010.09.007.

Ferreira, E.B., Cavalcanti, P.P., Nogueira, D.A., 2014. ExpDes: an R package for ANOVA and experimental designs. Appl. Math. 5, 2952.
Fu, Z., Wu, F., Song, K., Lin, Y., Bai, Y., Zhu, Y., Giesy, J.P., 2013. Competitive interaction between soil-derived humic acid and phosphate on goethite. Appl. Geochem. 36, 125–131. https://doi.org/10.1016/j.apgeochem.2013.05.015.
Gao, S., DeLuca, T.H., Cleveland, C.C., 2019. Biochar additions alter phosphorus and nitrogen availability in agricultural ecosystems: a meta-analysis. Sci. Total Environ. 654, 463–472. https://doi.org/10.1016/j.scitotenv.2018.11.124.
Geissler, B., Mew, M.C., Steiner, G., 2019. Phosphate supply security for importing countries: developments and the current situation. Sci. Total Environ. 677, 511–523.
Ghodszad, L., Reyhanitabar, A., Maghsoodi, M.R., Asgari Lajayer, B., Chang, S.X., 2021. Biochar affects the fate of phosphorus in soil and water: a critical review. Chemosphere 283, 131176. https://doi.org/10.1016/j.chemosphere.2021.131176.
Gimsing, A.L., Borggaard, O.K., Bang, M., 2004. Influence of soil composition on adsorption of glyphosate and phosphate by contrasting Danish surface soils. Eur. J. Soil Sci. 55, 183–191. https://doi.org/10.1046/j.1365-2389.2003.00585.x.
Glaser, B., Lehr, V.I., 2019. Biochar effects on phosphorus availability in agricultural soils: a meta-analysis. Sci. Rep. 9, 1–9. https://doi.org/10.1038/s41598-019-45693-z.
Gross, A., Bromm, T., Glaser, B., 2021. Soil organic carbon sequestration after biochar application: a global meta-analysis. Agronomy 11, 2474.
Guelfi, D., Nunes, A.P.P., Sarkis, L.F., Oliveira, D.P., 2022. Innovative phosphate fertilizer technologies to improve phosphorus use efficiency in agriculture. Sustainability 14. https://doi.org/10.3390/su142114266.
Inglezakis, V.J., Fyrillas, M.M., 2017. Adsorption fixed beds modeling revisited: generalized solutions for S-shaped isotherms. Chem. Eng. Commun. 204, 1299–1317.
Ippolito, J.A., Cui, L., Kammann, C., Wrage-Mönnig, N., Estavillo, J.M., Fuertes-Mendizabal, T., Cayuela, M.L., Sigua, G., Novak, J., Spokas, K., 2020. Feedstock choice, pyrolysis temperature and type influence biochar characteristics: a comprehensive meta-data analysis review. Biochar 2, 421–438.
Izhar Shafi, M., Adnan, M., Fahad, S., Wahid, F., Khan, A., Yue, Z., Danish, S., Zafar-ul-Hye, M., Brtnicky, M., Datta, R., 2020. Application of single superphosphate with humic acid improves the growth, yield and phosphorus uptake of wheat (Triticum aestivum L.) in calcareous soil. Agronomy 10, 1224.
Jing, J., Zhang, S., Yuan, L., Li, Y., Lin, Z., Xiong, Q., Zhao, B., 2020. Combining humic acid with phosphate fertilizer affects humic acid structure and its stimulating efficacy on the growth and nutrient uptake of maize seedlings. Sci. Rep. 10, 1–10.
Keiluweit, M., Nico, P.S., Johnson, M., Kleber, M., 2010. Dynamic molecular structure of plant biomass-derived black carbon (biochar). Environ. Sci. Technol. 44, 1247–1253. https://doi.org/10.1021/ES9031419/SUPPL_FILE/ES9031419_SI_001.PDF.
Kinney, T.J., Masiello, C.A., Dugan, B., Hockaday, W.C., Dean, M.R., Zygourakis, K., Barnes, R.T., 2012. Hydrologic properties of biochars produced at different temperatures. Biomass and Bioenergy 41, 34–43. https://doi.org/10.1016/j.biombioe.2012.01.033.
Kołodyńska, D., Krukowska, J., Thomas, P., 2017. Comparison of sorption and desorption studies of heavy metal ions from biochar and commercial active carbon. Chem. Eng. J. 307, 353–363. https://doi.org/10.1016/j.cej.2016.08.088.
Lagergren, S., 1898. Zur theorie der sogenannten adsorption gelöster stoffe, Kungliga Svenska Vetenskapsakademiens. Handlingar 24 (4), 1–39.
Laskosky, J.D., Mante, A.A., Zvomuya, F., Amarakoon, I., Leskiw, L., 2020. A bioassay of long-term stockpiled salvaged soil amended with biochar, peat, and humalite. Agrosystems, Geosci. Environ. 3, e20068.
Lehmann, J., Joseph, S., 2015. Biochar for Environmental Management.
Li, X., Qin, Y., Jia, Y., Li, Y., Zhao, Y., Pan, Y., Sun, J., 2021. Preparation and application of Fe/biochar (Fe-BC) catalysts in wastewater treatment: a review. Chemosphere 274, 129766.
Liou, T.-H., Wu, S.-J., 2009. Characteristics of microporous/mesoporous carbons prepared from rice husk under base- and acid-treated conditions. J. Hazard Mater. 171, 693–703. https://doi.org/10.1016/J.JHAZMAT.2009.06.056.
Lowell, S., Shields, J.E., Thomas, M.A., Thommes, M., 2006. Characterization of Porous solids and Powders: surface Area, Pore Size and Density. Springer Science & Business Media.
Luo, D., Wang, L., Nan, H., Cao, Y., Wang, H., Kumar, T.V., Wang, C., 2022. Phosphorus adsorption by functionalized biochar: a review. Environ. Chem. Lett. 1–28.
Lustosa Filho, J.F., Penido, E.S., Castro, P.P., Silva, C.A., Melo, L.C.A., 2017. Co-pyrolysis of poultry litter and phosphate and magnesium generates alternative slow-release fertilizer suitable for tropical soils. ACS Sustain. Chem. Eng. 5, 9043–9052. https://doi.org/10.1021/acssuschemeng.7b01935.
Lustosa Filho, J.F., Barbosa, C.F., Carneiro, J.S., da, S., Melo, L.C.A., 2019. Diffusion and phosphorus solubility of biochar-based fertilizer: visualization, chemical assessment and availability to plants. Soil Tillage Res. 194, 104298 https://doi.org/10.1016/j.still.2019.104298.
MacCarthy, P., Clapp, C.E., Bloom, P.R., Malcolm, R.L., 2015. Humic substances in soil and crop sciences: an overview. Humic Subst. Soil Crop Sci. Sel. Readings 261–271. https://doi.org/10.2136/1990.humicsubstances.c11.
MAPA - Ministério da Agricultura, Pecuária e Abastecimento, 2017. Manual de métodos analíticos oficiais para fertilizantes e corretivos. Brasília, DF. 240p.
McBeath, T.M., McLaughlin, M.J., Kirby, J.K., Armstrong, R.D., 2012. Dry soil reduces fertilizer phosphorus and zinc diffusion but not bioavailability. Soil Sci. Soc. Am. J. 76, 1301. https://doi.org/10.2136/sssaj2011.0431.
Melo, L.C.A., Lehmann, J., Carneiro, J.S., da, S., Camps-Arbestain, M., 2022. Biochar-based fertilizer effects on crop productivity: a meta-analysis. Plant Soil 472, 45–58. https://doi.org/10.1007/s11104-021-05276-2.
Mobed, et al., 2000. Fluorescence characterization of IHSS humic substances : total luminescence spectra with absorbance correction. Environ. Sci. Technol. 30, 3061–3065.
Morales, M.M., Comerford, N., Guerrini, I.A., Falcão, N.P.S., Reeves, J.B., 2013. Sorption and desorption of phosphate on biochar and biochar-soil mixtures. Soil Use Manag. 29, 306–314. https://doi.org/10.1111/sum.12047.
Nakarmi, A., Bourdo, S.E., Ruhl, L., Kanel, S., Nadagouda, M., Alla, P.K., Pavel, I., Viswanathan, T., 2020. Benign zinc oxide betaine-modified biochar nanocomposites for phosphate removal from aqueous solutions. J. Environ. Manag. 272, 111048.
Nguyen, T.B., Truong, Q.M., Chen, C.W., Doong, R. an, Chen, W.H., Dong, C. Di, 2022. Mesoporous and adsorption behavior of algal biochar prepared via sequential hydrothermal carbonization and ZnCl2 activation. Bioresour. Technol. 346, 126351 https://doi.org/10.1016/j.biortech.2021.126351.
Novais, R.F., Smyth, T.J., 1999. Fósforo em solo e planta em condições tropicais. Universidade Federal de Viçosa.
Novais, F.R., J, C.L.N., N, F.B., Oliveira, A.J., Garrido, W.E., Araújo, J.D., S, L., 1991. Métodos de Pesquisa Em Fertilidade Do Solo.
Pavinato, P.S., Rocha, G.C., Cherubin, M.R., Harris, I., Jones, D.L., Withers, P.J.A., 2020. Map of total phosphorus content in native soils of Brazil. Sci. Agric. 78, 1–5. https://doi.org/10.1590/1678-992x-2020-0077.
Perondi, D., Bassanesi, G.R., Manera, C., Lazzari, L.K., Godinho, M., Zattera, A.J., Dotto, G.L., 2021. From cellulose to graphene-like porous carbon nanosheets. Microporous Mesoporous Mater. 323, 111217.
Pierotti, R., Rouquerol, J., 1985. Reporting physisorption data for gas/solid systems with special reference to the determination of surface area and porosity. Pure Appl. Chem. 57, 603–619.
Pogorzelski, D., Filho, J.F.L., Matias, P.C., Santos, W.O., Vergütz, L., Melo, L.C.A., 2020. Biochar as composite of phosphate fertilizer: characterization and agronomic effectiveness. Sci. Total Environ. 743, 140604 https://doi.org/10.1016/j.scitotenv.2020.140604.
Pookmanee, P., Wannawek, A., Satienperakul, S., Putharod, R., Laorodphan, N., Sangsrichan, S., Phanichphant, S., 2016. Characterization of diatomite, leonardite and pumice. In: Materials Science Forum. Trans Tech Publ, pp. 211–215.
R Core Team, 2022. R: A Language and Environment for Statistical computing. R Foundation for Statistical Computing, Vienna, Austria.
Rajan, M., Shahena, S., Chandran, V., Mathew, L., 2021. Chapter 3 – controlled release of fertilizers – concept, reality, and mechanism. In: Lewu, F.B., Volova, T., Thomas, S., K, R.R. (Eds.), Controlled Release Fertilizers for Sustainable Agriculture. Academic Press, pp. 41–56. https://doi.org/10.1016/B978-0-12-819555-0.00003-0.
Regazzi, A.J., 1999. Teste para verificar a identidade de modelos de regressão e a igualdade de parâmetros no caso de dados de delineamentos experimentais. Ceres 46, 383–409.
Roberts, T.L., Johnston, A.E., 2015. Phosphorus use efficiency and management in agriculture. Resour. Conserv. Recycl. 105, 275–281. https://doi.org/10.1016/j.resconrec.2015.09.013.
Rose, T.J., Wissuwa, M., 2012. Chapter five – rethinking internal phosphorus utilization efficiency: a new approach is needed to improve PUE in grain crops. In: Sparks, D.L. (Ed.), Advances in Agronomy. Academic Press, pp. 185–217. https://doi.org/10.1016/B978-0-12-394277-7.00005-1.
Sahoo, T.R., Prelot, B., 2020. Chapter 7 – adsorption processes for the removal of contaminants from wastewater: the perspective role of nanomaterials and nanotechnology. In: Bonelli, B., Freyria, F.S., Rossetti, I., Sethi, R. (Eds.), Nanomaterials for the Detection and Removal of Wastewater Pollutants, Micro and Nano Technologies. Elsevier, pp. 161–222. https://doi.org/10.1016/B978-0-12-818489-9.00007-4.
Samoraj, M., Mironiuk, M., Witek-Krowiak, A., Izydorczyk, G., Skrzypczak, D., Mikula, K., Baśladyńska, S., Moustakas, K., Chojnacka, K., 2022. Biochar in environmental friendly fertilizers – prospects of development products and technologies. Chemosphere 296, 133975. https://doi.org/10.1016/j.chemosphere.2022.133975.
Sarlaki, E., Paghaleh, A.S., Kianmehr, M.H., Vakilian, K.A., 2021. Valorization of lignite wastes into humic acids: process optimization, energy efficiency and structural features analysis. Renew. Energy 163, 105–122.
Scherdel, C., Reichenauer, G., Wiener, M., 2010. Relationship between pore volumes and surface areas derived from the evaluation of N2-sorption data by DR-, BET- and t-plot. Microporous Mesoporous Mater. 132, 572–575.
Shi, Y., Yu, Y., Chang, E., Wang, R., Hong, Z., Cui, J., Zhang, F., Jiang, J., Xu, R., 2023. Effect of biochar incorporation on phosphorus supplementation and availability in soil: a review. J. Soils Sediments 23, 672–686. https://doi.org/10.1007/s11368-022-03359-w.
Sible, C.N., Seebauer, J.R., Below, F.E., 2021. Plant biostimulants: a categorical review, their implications for row crop production, and relation to soil health indicators. Agronomy 11, 1297.
Sims, J.T., Sharpley, A.N., Condron, L.M., Turner, B.L., Cade-Menun, B.J., 2005. Chemistry and Dynamics of Soil Organic Phosphorus. https://doi.org/10.2134/agronmonogr46.c4.
Song, Q., Zhao, H., Jia, J., Yang, L., Lv, W., Gu, Q., Shu, X., 2020. Journal of Analytical and Applied Pyrolysis Effects of demineralization on the surface morphology, microcrystalline and thermal transformation characteristics of coal. J. Anal. Appl. Pyrolysis 145, 104716. https://doi.org/10.1016/j.jaap.2019.104716.
Strawn, D.G., Sparks, D.L., 2000. Effects of soil organic matter on the kinetics and mechanisms of Pb(II) sorption and desorption in soil. Soil Sci. Soc. Am. J. 64, 144–156. https://doi.org/10.2136/sssaj2000.641144x.
Tesfaye, F., Liu, X., Zheng, J., Cheng, K., Bian, R., Zhang, X., Li, L., Drosos, M., Joseph, S., Pan, G., 2021. Could biochar amendment be a tool to improve soil availability and

plant uptake of phosphorus? A meta-analysis of published experiments. Environ. Sci. Pollut. Res. 28, 34108–34120. https://doi.org/10.1007/s11356-021-14119-7.

Tian, D., Xu, Z., Zhang, D., Chen, W., Cai, J., Deng, H., Sun, Z., Zhou, Y., 2019. Micro–mesoporous carbon from cotton waste activated by FeCl3/ZnCl2: preparation, optimization, characterization and adsorption of methylene blue and eriochrome black T. J. Solid State Chem. 269, 580–587. https://doi.org/10.1016/j.jssc.2018.10.035.

USDA, 2014. Keys to Soil Taxonomy. Government Printing Office.

Vance, C.P., Uhde-Stone, C., Allan, D.L., 2003. Phosphorus acquisition and use: critical adaptations by plants for securing a nonrenewable resource. New Phytol. 157, 423–447. https://doi.org/10.1046/j.1469-8137.2003.00695.x.

Vejan, P., Khadiran, T., Abdullah, R., Ahmad, N., 2021. Controlled release fertilizer : a review on developments, applications and potential in agriculture. J. Contr. Release 339, 321–334. https://doi.org/10.1016/j.jconrel.2021.10.003.

Volf, M.R., Rosolem, C.A., 2021. Soil P diffusion and availability modified by controlled-release P fertilizers. J. Soil Sci. Plant Nutr. 21, 162–172. https://doi.org/10.1007/S42729-020-00350-7/FIGURES/4.

Wang, H., Zhu, J., Fu, Q., Hong, C., Hu, H., Violante, A., 2016. Phosphate adsorption on uncoated and humic acid-coated iron oxides. J. Soils Sediments 16, 1911–1920. https://doi.org/10.1007/s11368-016-1383-8.

Withers, P.J.A., Rodrigues, M., Soltangheisi, A., De Carvalho, T.S., Guilherme, L.R.G., Benites, V.D.M., Gatiboni, L.C., De Sousa, D.M.G., Nunes, R.D.S., Rosolem, C.A., Andreote, F.D., Oliveira, A. De, Coutinho, E.L.M., Pavinato, P.S., 2018. Transitions to sustainable management of phosphorus in Brazilian agriculture. Sci. Rep. 8, 1–13. https://doi.org/10.1038/s41598-018-20887-z.

Xia, D., Tan, F., Zhang, C., Jiang, X., Chen, Z., Li, H., Zheng, Y., Li, Q., Wang, Y., 2016. Applied Surface Science ZnCl 2 -activated biochar from biogas residue facilitates aqueous as (III) removal. Appl. Surf. Sci. 377, 361–369. https://doi.org/10.1016/j.apsusc.2016.03.109.

Xu, J., Chen, L., Qu, H., Jiao, Y., Xie, J., Xing, G., 2014. Preparation and characterization of activated carbon from reedy grass leaves by chemical activation with H 3 PO 4. Appl. Surf. Sci. 320, 674–680. https://doi.org/10.1016/j.apsusc.2014.08.178.

Xu, J., Mohamed, E., Li, Q., Lu, T., Yu, H., Jiang, W., 2021. Effect of humic acid addition on buffering capacity and nutrient storage capacity of soilless substrates. Front. Plant Sci. 749.

Yan, L., Liu, Y., Zhang, Yudan, Liu, S., Wang, C., Chen, W., Liu, C., Chen, Z., Zhang, Ying, 2020. ZnCl2 modified biochar derived from aerobic granular sludge for developed microporosity and enhanced adsorption to tetracycline. Bioresour. Technol. 297, 122381 https://doi.org/10.1016/j.biortech.2019.122381.

Yang, F., Antonietti, M., 2020. The sleeping giant: a polymer view on humic matter in synthesis and applications. Prog. Polym. Sci. 100, 101182 https://doi.org/10.1016/j.progpolymsci.2019.101182.

Yang, C., Lu, S., 2022. Straw and straw biochar differently affect phosphorus availability, enzyme activity and microbial functional genes in an. Ultisol. Sci. Total Environ. 805, 150325 https://doi.org/10.1016/j.scitotenv.2021.150325.

Zavarzina, A.G., Danchenko, N.N., Demin, V.V., Artemyeva, Z.S., Kogut, B.M., 2021. Humic substances: hypotheses and reality (a review). Eurasian Soil Sci. 54, 1826–1854. https://doi.org/10.1134/S1064229321120164.

Zavaschi, E., de Abreu Faria, L., Ferraz-Almeida, R., do Nascimento, C.A.C., Pavinato, P. S., Otto, R., Vitti, A.C., Vitti, G.C., 2020. Dynamic of P Flux in tropical acid soils fertilized with humic acid–complexed phosphate. J. Soil Sci. Plant Nutr. 20, 1937–1948. https://doi.org/10.1007/s42729-020-00265-3.

Zhang, L., Loáiciga, H.A., Xu, M., Du, C., Du, Y., 2015. Kinetics and mechanisms of phosphorus adsorption in soils from diverse ecological zones in the source area of a drinking-water reservoir. Int. J. Environ. Res. Publ. Health 12, 14312–14326.

Zhao, L., Cao, X., Mašek, O., Zimmerman, A., 2013. Heterogeneity of biochar properties as a function of feedstock sources and production temperatures. J. Hazard Mater. 256, 1–9. https://doi.org/10.1016/j.jhazmat.2013.04.015.

Zhu, J., Li, M., Whelan, M., 2018. Phosphorus activators contribute to legacy phosphorus availability in agricultural soils: a review. Sci. Total Environ. 612, 522–537. https://doi.org/10.1016/j.scitotenv.2017.08.095.

Zou, T., Zhang, X., Davidson, E.A., 2022. Global trends of cropland phosphorus use and sustainability challenges. Nature 611, 81–87. https://doi.org/10.1038/s41586-022-05220-z.